JOURNAL OF COMPUTATIONAL PHYSICS **126,** 286–298 (1996)
ARTICLE NO. 0138

A Method for Determining the Velocity Induced by Highly Anisotropic Vorticity Blobs

J. S. MARSHALL* AND J. R. GRANT†

*Department of Mechanical Engineering and Iowa Institute of Hydraulic Research, The University of Iowa, Iowa City, Iowa 52242, and †Naval Undersea Warfare Center, Newport, Rhode Island 02841

Received November 14, 1994; revised September 18, 1995

Resolution of boundary layer flows at moderate or high Reynolds numbers with the vortex blob method requires a great many isotropic elements. In this paper, an approximate method for determination of the induced velocity from highly anisotropic vorticity blobs is presented, and issues related to use of anisotropic elements in calculations with vortex blob algorithms for high Reynolds number near-wall flows are examined. The method presented here can be used to determine the induced velocity from smooth blob functions of arbitrary form, provided that the vorticity length scale associated with the blob is much less in one direction than in orthogonal directions. The ratio of these length scales is called the blob aspect ratio, ε, and is used as a small parameter to construct an asymptotic approximation to the induced velocity field. This method is applied in the present paper to derive induced velocity expressions for anisotropic Gaussian blob functions in both two and three dimensions. It is argued, using test calculations for a Blasius boundary layer, that although direct calculation of the induced velocity requires about an order of magnitude more CPU time for anisotropic Gaussian elements than for isotropic elements, this difference is more than made up for by a reduction of several orders of magnitude in the number of elements needed to resolve boundary layer flows at moderate to high Reynolds numbers. It is also found that the standard vortex blob representation leads to errors in the calculation of wall slip velocity and wall shear stress due to smoothing of the discontinuity between the real and image vorticity fields at the wall, but that these errors can be avoided by placing doublet-type elements along the wall.

1. INTRODUCTION

Singular anisotropic vorticity elements, in the form of small vortex sheets typically aligned tangent to a nearby solid boundary, have been used for the calculation of flow in fluid boundary layers as far back as the seminal work of Chorin [1]. Because vortex sheets are consistent with the natural tendency of vorticity length scaling within boundary layers, fewer sheet-like elements are needed to achieve a given resolution in boundary layer flows than for similar calculations employing point singularities. However, singular elements tend to produce noisy surface pressure results and are unsuited to most deterministic diffusion schemes.

Non-singular vortex methods employing anisotropic elements with piece-wise constant vorticity distributions have been used by Teng [2] for elliptical elements and by Huyer *et al.* [3] for rectangular elements. Bernard [4] recently presented a method for boundary layer flows in which the velocity field is obtained by integrating over anisotropic rectangular vorticity tiles in which the vorticity varies within each tile but is discontinuous at the tile edges. While non-singular, but discontinuous, vorticity representations considerably lessen the noise problems experienced with singular representations, the contribution to velocity at a point due to nearby elements is still inaccurately estimated with these methods because the vorticity tiles in some places overlap and in other places separate to leave gaps between tiles.

Several recent vortex blob methods (e.g., Knio and Ghoniem [5], Winckelmans and Leonard [6], Koumoutsakos *et al.* [7]) avoid problems with singular and discontinuous vorticity fields by using a representation consisting of a set of smooth, overlapping vorticity "blobs," a popular example being the Gaussian distribution. In order for a vortex blob representation to be useful, it must be possible to determine the velocity induced by the vorticity element either analytically or using a minimum amount of numerical integration. Due to the difficulty in obtaining an analytical expression for induced velocity of a sufficiently smooth anisotropic element, previous calculations with smooth vorticity representations have relied on isotropic elements and have necessarily been limited to either two dimensions or low Reynolds numbers for near-wall viscous flow calculations.

In this paper, an approximate method for determination of the induced velocity from highly anisotropic, smooth vorticity elements is presented. The method is based on an asymptotic approximation which uses the element aspect ratio ε as a small parameter, where the maximum relative error in induced velocity field is of order ε. The method can be used to convert any of a variety of different isotropic blob functions (e.g., see Winckelmans and Leonard [6]) to anisotropic forms. To illustrate the method,

0021-9991/96 $18.00

explicit expressions are derived in the present paper for the case of Gaussian elements in both two and three dimensions.

Anisotropic vorticity elements can be used for computing near-surface flows either with the standard vortex blob algorithm [8, 9], after some extension of the convergence proofs, or with other algorithms based on a smooth vorticity representation (e.g., Marshall and Grant [10]). The use of anisotropic elements potentially offers an enormous speedup for calculations of moderate and high Reynolds number near-surface flows, since the vorticity field in the boundary layer can be covered (with a given resolution) using far fewer anisotropic elements than would be required for computations with isotropic elements. The reduction in number of elements also yields substantial memory savings, which is particularly important for calculations employing accelerated algorithms (e.g., Greengard and Rokhlin [11]). The velocity induced by anisotropic vorticity doublets, for which the sign of the vorticity is opposite in the two halves of the element, is obtained by a similar asymptotic method. It is shown in the present paper that the standard vortex blob representation can lead to significant error in boundary layer flows in calculation of slip velocity and wall shear stress, but that these errors can be avoided by placing vorticity doublets along the wall.

Some background and a general summary of the asymptotic method to be followed is given in Section 2. The method is then illustrated for two- and three-dimensional Gaussian elements in Sections 3 and 4, respectively, including evaluation of the relative time requirement for velocity calculation using anisotropic Gaussian elements in comparison to that for isotropic elements. The computational savings attainable with use of anisotropic elements are documented in Section 5 using calculations for velocity profile in a Blasius boundary layer for both isotropic and anisotropic Gaussian elements. The variation of error in resolution of the velocity profile with the number of elements is also discussed in this section, with particular emphasis on satisfaction of the no-slip condition at the wall. In Section 6, induced velocity expressions for vorticity doublets are obtained using a formulation similar to that presented in Section 3, and it is shown that excellent reproduction of the Blasius boundary layer profile can be obtained, even with rather few elements, by placing anisotropic vorticity doublets along the wall, together with anisotropic blobs in the boundary layer. Some conclusions are given in Section 7.

2. GENERAL BACKGROUND AND OVERVIEW OF ASYMPTOTIC METHOD

The velocity vector $\mathbf{u}$ in an incompressible flow can be decomposed, in the usual way, as the sum of the curl of a vector potential $\boldsymbol{\psi}$ and an irrotational flow. Since in the usual vortex blob method the boundary conditions on the surface of solid bodies present in the flow are enforced using a panel method (rather than through a choice of the blob function), we can omit the irrotational part of this decomposition for the present and consider only the induced velocity field of the element in an unbounded domain, such that

$$\mathbf{u} = \nabla \times \boldsymbol{\psi}. \tag{1}$$

Since $\boldsymbol{\psi}$ is divergence-free, the vorticity $\boldsymbol{\omega}$ is related to $\boldsymbol{\psi}$ by the vector Poisson equation

$$\boldsymbol{\omega} \equiv \nabla \times \mathbf{u} = -\nabla^2 \boldsymbol{\psi}. \tag{2}$$

The particular solutions for $\boldsymbol{\psi}$ and $\mathbf{u}$ have the well-known forms

$$\begin{aligned} \boldsymbol{\psi}(\mathbf{x}, t) &= \frac{1}{4\pi} \int_V \frac{\boldsymbol{\omega}(\mathbf{x}', t)}{r}\, dv, \\ \mathbf{u}(\mathbf{x}, t) &= -\frac{1}{4\pi} \int_V \frac{\mathbf{r} \times \boldsymbol{\omega}(\mathbf{x}', t)}{r^3}\, dv \end{aligned} \tag{3a}$$

in three dimensions and

$$\begin{aligned} \boldsymbol{\psi}(\mathbf{x}, t) &= -\frac{1}{2\pi} \int_A \boldsymbol{\omega}(\mathbf{x}', t) \ln(r)\, da, \\ \mathbf{u}(\mathbf{x}, t) &= -\frac{1}{2\pi} \int_A \frac{\mathbf{r} \times \boldsymbol{\omega}(\mathbf{x}', t)}{r^2}\, da \end{aligned} \tag{3b}$$

in two dimensions.

In two dimensions all vorticity fields are divergence-free, but in three-dimensional problems the choice of vorticity element is restricted by the kinematic requirement that the vorticity field have vanishing divergence. As noted by Novikov [12] and Winckelmans and Leonard [6], the solution $(3b)_2$ for induced velocity is unchanged if we replace the vorticity $\boldsymbol{\omega}$ in this expression with a vector field $\mathbf{q}$ (which we will call the *generator field*), that differs from the vorticity by the gradient of a scalar. Writing

$$\mathbf{q} = \boldsymbol{\omega} + \nabla \phi \tag{4}$$

and taking the divergence gives a Poisson equation for ϕ as

$$\nabla^2 \phi = \nabla \cdot \mathbf{q}. \tag{5}$$

An expression for ϕ can be obtained either by solving the Poisson equation (5) using Green's functions or by solving (4) for $\boldsymbol{\omega}$, substituting into (3b), and taking the curl of the

resulting equation. The solution for ϕ can be written, after using various vector identities, in the form

$$\phi(\mathbf{x}, t) = \frac{1}{4\pi} \int_V \frac{\mathbf{r} \cdot \mathbf{q}(\mathbf{x}', t)}{r^3} \, dv. \tag{6}$$

Substituting (6) into (4) and solving for $\boldsymbol{\omega}$ gives the vorticity field in terms of the generator field. The $\nabla\phi$ term in (4) makes a contribution to the vector potential in $(3b)_1$ which can similarly be written as the gradient of a scalar, or

$$\boldsymbol{\psi} = \boldsymbol{\eta} + \nabla\sigma, \tag{7}$$

where the $\nabla\sigma$ term in (7) does not contribute to the induced velocity and $\boldsymbol{\eta}$ is determined only by the generator field $\mathbf{q}$ from

$$\nabla^2 \boldsymbol{\eta} = -\mathbf{q}. \tag{8}$$

A representation for the generator field is now introduced in terms of N overlapping anisotropic elements, located at control points $\mathbf{x}_n(t)$ and having radii $R_n(t)$ and aspect ratios $\varepsilon_n(t)$, as

$$\mathbf{q}(\mathbf{x}, t) = \sum_{n=1}^{N} \boldsymbol{\Omega}_n(t) \, f_n(\mathbf{x} - \mathbf{x}_n, R_n, \varepsilon_n). \tag{9}$$

The element weighting functions (or "blob functions") f_n are normalized by

$$\int_V f_n \, dv = 1, \tag{10}$$

so that the amplitude $\boldsymbol{\Omega}_n$ is equal to the integral of the vorticity contained in element n over all space. The part $\boldsymbol{\eta}$ of the vector potential and the induced velocity $\mathbf{u}$ are obtained by substituting (9) into integrals similar to (3a) and (3b), with $\boldsymbol{\omega}$ replaced by $\mathbf{q}$ and $\boldsymbol{\psi}$ replaced by $\boldsymbol{\eta}$. Since these equations are linear in $\mathbf{q}$, the induced velocities and vector potentials evaluated from each element can be added to give the total values at any point.

By writing a representation for the generator field (rather than for the total vorticity field) for three-dimensional problems, the requirement of divergence-free vorticity can always be enforced. We will follow this approach, for notational convenience, in both two and three dimensions in the rest of this section, where for two dimensions it is implicit that ϕ vanishes everywhere. In traditional vortex algorithms [6–10], the generator field $\mathbf{q}$ is also used in the equations of motion in place of the vorticity $\boldsymbol{\omega}$; however, Marshall and Grant [10] have recently presented an approach by which it is possible to evolve the total vorticity $\boldsymbol{\omega}$ on the control points while still using a representation of the form (9) for $\mathbf{q}$.

We now consider the velocity induced by a single element of unit amplitude $\mathbf{a}$ and write the generator field for this element as

$$\mathbf{q} = A h(\mathbf{x}) \, \mathbf{a}. \tag{11}$$

Since the equation (8) that we wish to solve does not explicitly involve time, time dependence will not be explicitly denoted in the following. In (11), $\mathbf{a}$ is a unit vector which specifies the direction of $\mathbf{q}$ and the blob function has been written as the product of a vorticity distribution function $h(\mathbf{x})$ and a normalization constant A. From the normalization condition (10), the constant A is obtained as

$$A \int_V h(\mathbf{x}) \, dv = 1. \tag{12}$$

We consider a solution of (8) in which $\boldsymbol{\eta}$ is in the same direction $\mathbf{a}$ as the generator field, so that

$$\boldsymbol{\eta} = -\left(\frac{A}{\beta}\right) I(\mathbf{x}) \, \mathbf{a}, \tag{13}$$

where the constant β equals 2π in two dimensions and 4π in three dimensions. Substituting (11) and (13) into (8) gives a scalar Poisson equation for the function I of the form

$$\nabla^2 I = \beta \, h(\mathbf{x}). \tag{14}$$

The approximate method for solution of (14) to be followed in the paper is summarized here for the case of two-dimensional flows in the $x - y$ plane. It is assumed that the distribution function $h(\mathbf{x})$ is symmetric with respect to both the x and y axes. The solution $I(\mathbf{x})$ of (14) will then satisfy the symmetry conditions

$$\begin{aligned} &\frac{\partial I}{\partial x}(-x, y) = -\frac{\partial I}{\partial x}(x, y), \quad \frac{\partial I}{\partial x}(x, -y) = \frac{\partial I}{\partial x}(x, y), \\ &\frac{\partial I}{\partial y}(-x, y) = \frac{\partial I}{\partial y}(x, y), \quad \frac{\partial I}{\partial y}(x, -y) = -\frac{\partial I}{\partial y}(x, y). \end{aligned} \tag{15}$$

Using (15), the solution for $I(x, y)$ can then be obtained in the positive $x - y$ quadrant subject to the boundary conditions

$$\left.\frac{\partial I}{\partial x}\right|_{x=0} = 0, \quad \left.\frac{\partial I}{\partial y}\right|_{y=0} = 0. \tag{16}$$

The function $I(x, y)$ in (14) can be written as the sum of some harmonic function $I_1(x, y)$ and a particular solution $I_2(x, y)$, such that

$$\nabla^2 I_1 = 0, \quad \nabla^2 I_2 = \beta h(x, y). \tag{17}$$

Let us now suppose that the distribution function $h(\mathbf{x})$ is prescribed such that the length scale in the y-direction is smaller by a factor $\varepsilon \ll 1$ than that in the x-direction. The particular solution I_2 will then be such that the second derivative with respect to x in $(17)_2$ will be smaller than that with respect to y by a factor of order ε^2. We can thus approximate $(17)_2$ by

$$\frac{\partial^2 I_2}{\partial y^2} = \beta h(x, y) + O(\varepsilon^2). \tag{18}$$

Integrating (18) twice with respect to y and using the fact that I_2 and its derivatives must approach zero at infinity yields a solution of the form

$$I_2(x, y) = \int_y^\infty \int_{y'}^\infty \beta h(x, y'')\, dy''\, dy'. \tag{19}$$

Differentiating (19) with respect to x, we see that the boundary condition $(16)_1$ on $x = 0$ is satisfied independently by I_2. Differentiating (19) with respect to y and setting $y = 0$ gives

$$\left.\frac{\partial I_2}{\partial y}\right|_{y=0} = -\int_0^\infty \beta h(x, y')\, dy'. \tag{20}$$

The integral on the right-hand side of (20) in general does not vanish, and so the part I_2 of $I(x, y)$ does not independently satisfy the boundary condition $(16)_2$ on $y = 0$. In order that (16) will be satisfied for the function $I(x, y)$ as a whole, we must seek a harmonic function I_1 which satisfies the boundary conditions

$$\left.\frac{\partial I_1}{\partial x}\right|_{x=0} = 0, \quad \left.\frac{\partial I_1}{\partial y}\right|_{y=0} = -\left.\frac{\partial I_2}{\partial y}\right|_{y=0} = \int_0^\infty \beta h(x, y')\, dy', \tag{21}$$

together with the requirement that the induced velocity reduce to that from a point vortex of unit circulation at infinity. Since the solution space for (17) is unbounded in the positive x and y directions, the solution for I_1 is most easily obtained using a transform method, as illustrated in the next two sections.

3. ANISOTROPIC GAUSSIAN ELEMENTS IN TWO DIMENSIONS

In this section, we use the method sketched in Section 2 to obtain an expression for the velocity induced by anisotropic Gaussian elements in two dimensions. While we present results for the popular Gaussian form, an algebraic expression for $h(x, y)$ may lead to even simpler forms for the relations arrived at below.

The distribution function $h(x, y)$ for the Gaussian element is written in terms of length variables x and y, which have been made dimensionless by division by the element radius R, as

$$h(x, y) = \exp[-(x^2 + y^2/\varepsilon^2)]. \tag{22}$$

Substituting (22) into (12) and performing the integration, the normalization constant A is obtained as

$$A = \frac{1}{\pi \varepsilon R^2}. \tag{23}$$

Now substituting (22) into (19) and performing the double integration over y, we obtain the particular solution I_2 of (14) as

$$I_2(x, y) = -\pi \varepsilon^2 e^{-x^2}\left[\sqrt{\pi}\frac{y}{\varepsilon}\operatorname{erfc}\left(\frac{y}{\varepsilon}\right) - e^{-y^2/\varepsilon^2}\right]. \tag{24}$$

Substitution of (24) and (22) into $(17)_2$ verifies that the maximum relative error in $\nabla^2 I_2$ is of $O(\varepsilon^2)$.

We now seek a harmonic function I_1 that satisfies the boundary conditions (21), where

$$\left.\frac{\partial I_1}{\partial y}\right|_{y=0} = -\left.\frac{\partial I_2}{\partial y}\right|_{y=0} = \pi^{3/2}\varepsilon e^{-x^2}. \tag{25}$$

A harmonic function $I_1(x, y)$ which satisfies $(21)_1$ identically can be written in terms of the Fourier cosine integral as

$$I_1(x, y) = C \ln(r) + \int_0^\infty f(k)\, e^{-ky} \cos(kx)\, dk, \tag{26}$$

where C is a constant to be determined and $r = (x^2 + y^2)^{1/2}$. The first term on the right-hand side in (26) represents a point vortex and thus satisfies $(17)_1$ and both of the boundary conditions (16) identically. Substituting (26) into the boundary condition (25) along $y = 0$, an integral equation for the function $f(k)$ in (26) is obtained as

$$\int_0^\infty k f(k) \cos(kx)\, dk = -\pi^{3/2}\varepsilon e^{-x^2}. \tag{27}$$

We note that the treatment of other distribution functions in two dimensions would be essentially the same as given above for the Gaussian, except that the functional dependence on x on the right-hand side of (27) would be different.

It now remains only to determine the function $f(k)$ and the constant C, subject to satisfaction of (27) and the boundary condition at infinity. To solve for $f(k)$, it is convenient to define a function $g(x)$ by

$$g(x) \equiv \int_0^\infty f(k) \sin(kx)\, dk, \tag{28}$$

such that (27) can be written as

$$\frac{\partial g}{\partial x} = -\pi^{3/2} \varepsilon\, e^{-x^2}. \tag{29}$$

In the case of Gaussian blobs, the solution for $f(k)$ can be obtained most easily by using properties of Fourier transforms, rather than by direct integration of (29). We recall the Fourier sine and cosine transform pairs

$$\begin{aligned} s(\omega) &= \sqrt{2/\pi} \int_0^\infty f(x) \sin(\omega x)\, dx, \\ f(x) &= \sqrt{2/\pi} \int_0^\infty s(\omega) \sin(\omega x)\, d\omega, \end{aligned} \tag{30a}$$

and

$$\begin{aligned} c(\omega) &= \sqrt{2/\pi} \int_0^\infty f(x) \cos(\omega x)\, dx, \\ f(x) &= \sqrt{2/\pi} \int_0^\infty c(\omega) \cos(\omega x)\, d\omega. \end{aligned} \tag{30b}$$

Using the property that

$$\int_0^\infty \frac{\partial g}{\partial x} \sin(\alpha x)\, dx = -\alpha \int_0^\infty g(x) \cos(\alpha x)\, dx \tag{31}$$

if $g(x) \to 0$ as $x \to \infty$ and taking the Fourier sine transform of (29), we obtain

$$\sqrt{2/\pi} \int_0^\infty g(x) \cos(\alpha x)\, dx = \sqrt{2}\, \pi \varepsilon \int_0^\infty e^{-x^2} \frac{\sin(\alpha x)}{\alpha}\, dx. \tag{32}$$

Taking the Fourier cosine transform of (32) and then taking the Fourier sine transform of the resulting equation, after substituting (28), gives

$$f(k) = \frac{4}{\sqrt{\pi}} \varepsilon \int_0^\infty \int_0^\infty \int_0^\infty e^{-\xi^2} \frac{\sin(\alpha\xi) \cos(\alpha\eta) \sin(k\eta)}{\alpha}\, d\xi\, d\alpha\, d\eta. \tag{33}$$

Using integrals number 3.741.2 and 3.896.4 of Gradshteyn and Ryzhik [13], (33) can be reduced to simply

$$f(k) = \frac{\pi\varepsilon}{k}(1 - e^{-k^2/4}). \tag{34}$$

Substituting (34) into (26) and taking derivatives with respect to x and y gives

$$\begin{aligned} \frac{\partial I_1}{\partial x} &= \frac{Cx}{r^2} - \pi\varepsilon \int_0^\infty (1 - e^{-k^2/4})\, e^{-ky} \sin(kx)\, dk, \\ \frac{\partial I_1}{\partial y} &= \frac{Cy}{r^2} - \pi\varepsilon \int_0^\infty (1 - e^{-k^2/4})\, e^{-ky} \cos(kx)\, dk, \end{aligned} \tag{35}$$

Using integrals number 3.897.1, 3.897.2, 3.893.1, and 3.893.2 of Gradshteyn and Ryzhik [13], the derivatives in (35) can be written in terms of the Faddeeva function [14] $w(z) \equiv e^{-z^2} \operatorname{erfc}(-iz)$, where $z = x + iy$, as

$$\begin{aligned} \frac{\partial I_1}{\partial x} &= (C - \pi\varepsilon) \frac{x}{x^2 + y^2} - \frac{\pi^{3/2} i\varepsilon}{2} [w(z) - w(-\bar{z})], \\ \frac{\partial I_1}{\partial y} &= (C - \pi\varepsilon) \frac{y}{x^2 + y^2} + \frac{\pi^{3/2}\varepsilon}{2} [w(z) + w(-\bar{z})], \end{aligned} \tag{36}$$

where an overbar denotes the complex conjugate.

The far-field expansion of the expressions (36) is simply

$$\frac{\partial I_1}{\partial x} = \frac{Cx}{x^2 + y^2}, \quad \frac{\partial I_2}{\partial y} = \frac{Cy}{x^2 + y^2}. \tag{37}$$

From the requirement that the induced velocity should approach that due to a point vortex with unit circulation sufficiently far away from the origin, we must choose the constant C as

$$C = \pi\varepsilon. \tag{38}$$

Gathering the results in (24), (26), (34), and (38), and neglecting $\partial I_2/\partial x$ which is everywhere smaller than the other terms by a factor of $O(\varepsilon)$ or less, the derivatives of I with respect to x and y can be written in terms of the real part a and the imaginary part b of $w(z)$ as

$$\frac{\partial I}{\partial x} = \pi^{3/2}\varepsilon b, \quad \frac{\partial I}{\partial y} = \pi^{3/2}\varepsilon a - \pi^{3/2}\varepsilon e^{-x^2} \operatorname{erfc}(y/\varepsilon). \tag{39}$$

The approximate solution (39) satisfies the boundary conditions at $x = 0$ and $y = 0$ identically, approaches the expected far-field form, and satisfies the differential equation (14) approximately with a relative error in $\nabla^2 I$ of at most $O(\varepsilon^2)$ for all x and y. The induced velocity field from

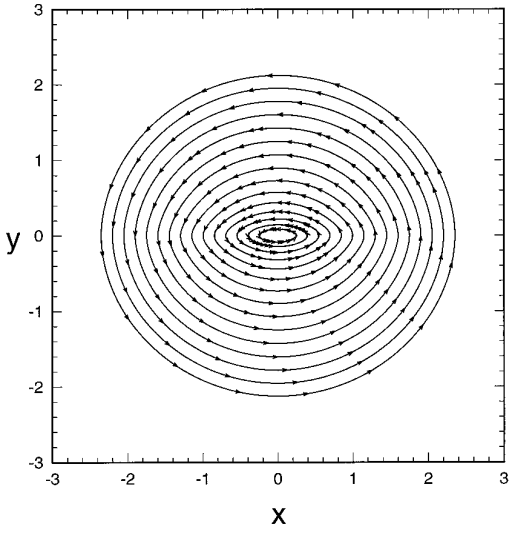

FIG. 1. Streamlines for a two-dimensional anisotropic Gaussian vorticity blob with aspect ratio $\varepsilon = 0.1$ and radius $R = 1$.

the single element is obtained in terms of the gradients in (39), using (1) and (13), as

$$u = -\frac{1}{2\varepsilon\pi^2}\frac{\partial I}{\partial y}, \quad v = \frac{1}{2\varepsilon\pi^2}\frac{\partial I}{dx}, \tag{40}$$

where u and v are non-dimensionalized by the element circulation divided by the element radius R.

A subroutine for efficient calculation of the function $w(z)$ is available [15]. (The potential user is warned, however, that this subroutine is subject to underflow errors for small values of y.) An example showing the streamlines of the induced velocity field from a Gaussian blob with aspect ratio $\varepsilon = 0.1$ is given in Fig. 1. Data on the maximum difference between the induced velocity from an anisotropic element and a point vortex is given in Table I as a function of distance away from the vortex center. The induced velocity field is nearly the same for all (small) values of the aspect ratio ε, with the exception that the curvature along the line $y = 0$ of the streamlines near the center of the vortex becomes increasingly sharper as ε decreases.

TABLE I

Data Showing the Difference between the Induced Velocity of a Two-Dimensional Gaussian Anisotropic Element (with $\varepsilon = 0.1$) and a Point Vortex of the Same Circulation for Different Numbers of Element Radii away from the Vortex Center

Number of element radii away from the vortex center	Maximum relative difference between induced velocity from anisotropic blob and point vortex
2	0.11
3	0.054
4	0.031
5	0.020
6	0.014
8	0.0078
10	0.0050

For an isotropic Gaussian element of unit circulation, the velocity is also given by (40) with the gradients of I given simply by

$$\frac{\partial I}{\partial x} = \frac{\pi\varepsilon\, x}{\rho^2}(1 - e^{-\rho^2}), \quad \frac{\partial I}{\partial y} = \frac{\pi\varepsilon\, y}{\rho^2}(1 - e^{-\rho^2}), \tag{41}$$

where $\rho = (x^2 + y^2)^{1/2}$. The average CPU time required for calculation of the velocity field induced from an anisotropic Gaussian element from (39)–(40) was found to be 9.3 times longer than that required for a Gaussian isotropic element from (40)–(41).

4. ANISOTROPIC GAUSSIAN ELEMENTS IN THREE DIMENSIONS

In three dimensions the distribution function for a Gaussian element is written in terms of a radial coordinate ρ ($\equiv\{x^2 + y^2\}^{1/2}$) and an axial coordinate z, where both ρ and z are made dimensionless by division by the element radius R, as

$$h(\rho, z) = \exp[-(\rho^2 + z^2/\varepsilon^2)]. \tag{42}$$

The normalization constant A is obtained from the integral (12) as

$$A = \frac{1}{\pi^{3/2}\varepsilon R^3}. \tag{43}$$

Since $h(\rho, z)$ is symmetric about the $\rho = 0$ axis and also symmetric about the plane $z = 0$, the function $I(\rho, z)$ satisfies the symmetry conditions

$$\frac{\partial I}{\partial \rho}(\rho, -z) = \frac{\partial I}{\partial \rho}(\rho, z), \quad \frac{\partial I}{\partial z}(\rho, -z) = -\frac{\partial I}{\partial z}(\rho, z), \tag{44}$$

so we only need to consider solution of (17) in the half-space $z > 0$, subject to the boundary conditions

$$\left.\frac{\partial I}{\partial \rho}\right|_{\rho=0} = 0, \quad \left.\frac{\partial I}{\partial z}\right|_{z=0} = 0. \tag{45}$$

The particular solution I_2 of $I(\rho, z)$ from (14) approximately satisfies an equation of the form (18), with (x, y) replaced by (ρ, z), respectively. Substituting the Gaussian

distribution function (42) and integrating twice over z gives the particular solution as

$$I_2 = -2\pi\varepsilon^2 e^{-\rho^2}\left[\sqrt{\pi}\frac{z}{\varepsilon}\operatorname{erfc}\left(\frac{z}{\varepsilon}\right) - e^{-z^2/\varepsilon^2}\right]. \quad (46)$$

The expression (46) for I_2 satisfies the first of (45), but not the second boundary condition on $z = 0$ or the far-field condition. We thus seek a harmonic function I_1 which satisfies the far-field condition and the boundary conditions

$$\left.\frac{\partial I_1}{\partial \rho}\right|_{\rho=0} = 0, \quad \left.\frac{\partial I_1}{\partial z}\right|_{z=0} = -\left.\frac{\partial I_2}{\partial z}\right|_{z=0} = 2\pi^{3/2}\varepsilon e^{-\rho^2}. \quad (47)$$

A harmonic function I_1 which satisfies $(47)_1$ identically is given by the integral

$$I_1(\rho, z) = \int_0^\infty f(k) e^{-kz} J_0(k\rho)\, dk, \quad (48)$$

where $J_0(\cdot)$ is the Bessel function of the first kind of order zero. The function $f(k)$ is chosen to satisfy the boundary condition $(47)_2$, such that using (48) we have

$$\int_0^\infty k f(k) J_0(k\rho)\, dk = -2\pi^{3/2}\varepsilon e^{-\rho^2}. \quad (49)$$

For other forms of blob functions in three dimensions, the general expression for I_1 would be similar to that given above, but the right-hand side of (49) would differ. Recalling the Hankel transform pair

$$\begin{aligned} h(\omega) &= \int_0^\infty x f(x) J_0(\omega x)\, dx, \\ f(x) &= \int_0^\infty \omega h(\omega) J_0(\omega x)\, d\omega, \end{aligned} \quad (50)$$

we take the inverse Hankel transform of (49) to obtain an expression for $f(k)$ as

$$f(k) = -2\pi^{3/2}\varepsilon \int_0^\infty \xi e^{-\xi^2} J_0(k\xi)\, d\xi. \quad (51)$$

Using integral number 6.614.1 and expression 8.485 in Gradshteyn and Ryzhik [13], as well as an identity in Abramowitz and Stegun [16], the integral in (51) can be solved to yield simply

$$f(k) = -\pi^{3/2}\varepsilon e^{-k^2/4}. \quad (52)$$

Combining (46), (48), and (52), an approximate expression for the derivatives of $I(\rho, z)$, with relative error of order ε, is given by

$$\frac{\partial I}{\partial \rho} = \pi^{3/2}\varepsilon \int_0^\infty k e^{-kz} e^{-k^2/4} J_1(k\rho)\, dk, \quad (53a)$$

$$\frac{\partial I}{\partial z} = -2\pi^{3/2}\varepsilon e^{-\rho^2}\operatorname{erfc}(z/\varepsilon) + \pi^{3/2}\varepsilon \int_0^\infty k e^{-kz} e^{-k^2/4} J_0(k\rho)\, dk. \quad (53b)$$

The solution (53) satisfies the boundary conditions on $\rho = 0$ and $z = 0$ identically, approaches the expected far-field solution and satisfies the differential equation (14) approximately with relative error of $O(\varepsilon^2)$ for all ρ and z. The velocity induced by the element can be obtained from these gradients, using (1) and (13), as

$$\mathbf{u} = -\frac{1}{4\pi^{5/2}\varepsilon}\nabla I \times \mathbf{a}, \quad (54)$$

where $\mathbf{u}$ is non-dimensionalized by the integral of vorticity over the element (the element amplitude) divided by the square of the element radius R.

We have not been able to obtain an analytical solution for the remaining integrals in (53), but instead we evaluate these integrals numerically using a Gauss–Laguerre quadrature of the form

$$\int_0^\infty f(\alpha) e^{-\alpha}\, d\alpha \cong \sum_{i=1}^N f(\alpha_i) w_i. \quad (55)$$

The optimal choices for evaluation points α_i and weighting functions w_i were obtained using an algorithm given by Press *et al.* [17]. For efficient evaluation of the integrals in (53a), (53b), the domain of numerical integration over k is divided into four regions based on the value of $|z|$. In region 1 (for $|z| \le z_{\text{small}}$), the integrals are approximated through $O(z)$ using the first few terms of the expansion $e^{-kz} = 1 - kz + \frac{1}{2}k^2z^2 + O(kz)^3$, which gives

$$\begin{aligned} \frac{\partial I}{\partial \rho} &\cong \pi^2\varepsilon\rho e^{-\rho^2}[I_0(\rho^2/2) - I_1(\rho^2/2)] - 4\pi^{3/2}\varepsilon\rho z e^{-\rho^2}, \\ \frac{\partial I}{\partial z} &\cong 2\pi^{3/2}\varepsilon e^{-\rho^2}\operatorname{erf}(z/\varepsilon) - \pi^{3/2}\varepsilon z \int_0^\infty k^2 \varepsilon^{-k^2/4} J_0(k\rho)\, dk, \end{aligned} \quad (56)$$

where $I_n(\cdot)$ is the modified Bessel function of order n of the first kind. The last term in $(56)_2$ can be evaluated using the Gauss–Laguerre sum (55) with $\alpha = k^2/4$ and $f(\alpha) = 4\sqrt{\alpha} J_0(2\rho\sqrt{\alpha})$.

For region 2 ($z_{\text{small}} \le |z| \le z_{\text{mid}}$), the integrals in (53) are directly computed using (55) with $\alpha = k^2/4$ and $f(\alpha)$

$= 2\ \exp(-2z\sqrt{\alpha})\ J_n(2\rho\sqrt{\alpha})$, where the order n of the Bessel function corresponds to the appropriate order in (53). From various test cases with similar integrals that admit an exact solution, it is found that the Gauss–Laguerre approximation converges most rapidly when the exponential term on the right-hand side of (55) decays faster than the function $f(\alpha)$. Thus, as z becomes larger, the e^{-kz} factor in (53) will initially decay faster than the $e^{-k^2/4}$ factor. In region 3 ($z_{\text{mid}} \le |z| \le z_{\text{big}}$), we thus again use the Gauss–Laguerre formula (55), but now set $\alpha = kz$ and $f(\alpha) = (\alpha/z^2)\ \exp(-\alpha^2/4z^2)\ J_n(\alpha\rho/z)$. In region 4 ($|z| \ge z_{\text{big}}$), the field point is sufficiently far away from the centroid that we can use the far-field expansions

$$\frac{\partial I}{\partial \rho} = \frac{\pi^{3/2}\varepsilon\rho}{(z^2+\rho^2)^{3/2}}, \quad \frac{\partial I}{\partial z} = \frac{\pi^{3/2}\varepsilon\, z}{(z^2+\rho^2)^{3/2}}. \tag{57}$$

The accuracy of our integration schemes can be assessed by comparing results obtained with different methods at a given point. For simplicity, these comparisons were performed in the $y = 0$ plane, so that $\rho = x$, and with the generator vector oriented in the y-direction. As an example, when the methods used in regions 2 and 3 are both applied at the point $x = z = -1.09$ with $N = 40$ in (55), the induced velocity predictions differ by only 0.6%. At a point $x = z = -1.98$ with a larger value of z (with $N = 40$), the induced velocity predictions differ by about 3%. Although the results are not very sensitive to the value of z_{mid} chosen, it is found that if the approach in region 3 is used for $|z|$ less than about 0.4, the results are very poor (and, in fact, qualitatively incorrect). Thus we must require that either z_{mid} or z_{small} be greater than or equal to 0.4. The predictions using the expansion in region 1 were compared with the numerical calculations in region 2, and the induced velocity predictions differ by about 10% for $x = z = -0.20$ and by about 3.7% for $x = z = -0.12$. Based on these comparisons, reasonable values for the borders between the different regions would seem to be given by choosing

$$z_{\text{small}} = 0.1, \quad z_{\text{mid}} = 0.5, \quad z_{\text{big}} = 4. \tag{58}$$

The values (58) are used, with $N = 40$, to obtain the streamlines for the velocity field in the $x - z$ plane shown in Fig. 2, for a case where the generator field is oriented along the y-direction.

Tests were also performed to examine the convergence rate of the Gauss–Laguarre integration by comparing predicted values for induced velocity for several different values of N in (55). For the approach used in region 3, it is found that the induced velocities do not change to within four significant figures for $N \ge 10$. In fact, even runs with $N = 5$ yield results which differ from those with higher values of N by less than 0.1%. For the approach used in region 2, the results also do not vary to within four significant figures for $N \ge 10$ at small values of ρ (e.g., $\rho = 0.20$). On the other hand, for large values of ρ in region 2 (e.g., $\rho = 4$), the results are quite poor for small values of N and it is recommended that $N \ge 40$ be chosen at such points to obtain acceptable accuracy.

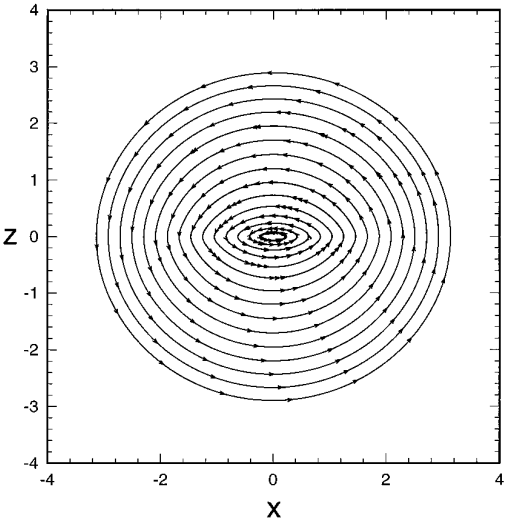

FIG. 2. Streamlines for a cross section on the $y = 0$ plane of a three-dimensional anisotropic Gaussian vorticity blob with amplitude aligned in the positive y-direction, aspect ratio $\varepsilon = 0.1$, and radius $R = 1$.

The induced velocity expression for an isotropic Gaussian element is given by (54) with the gradients of I given by

$$\frac{\partial I}{\partial \rho} = \frac{\pi^{3/2}\varepsilon\rho}{r^3} P\left(\frac{3}{2}, r^2\right), \quad \frac{\partial I}{\partial z} = \frac{\pi^{3/2}\varepsilon z}{r^3} P\left(\frac{3}{2}, r^2\right), \tag{59}$$

where $r = (z^2 + \rho^2)^{1/2}$ and P is the incomplete gamma function. Using an identity in Abramowitz and Stegun [16], we can relate $P(\frac{3}{2}, r^2)$ to the error function as

$$P\left(\frac{3}{2}, r^2\right) = \text{erf}\,(r) - \frac{2r\, e^{-r^2}}{\sqrt{\pi}}. \tag{60}$$

The CPU time required for numerical calculation of the induced velocity of a three-dimensional anisotropic Gaussian element at a point in regions 2 or 3 was found to be approximately equal to the number of terms N in the Gauss–Laguerre integration formula (55) times the CPU time required to compute induced velocity for an isotropic element. It is thus important to use no more terms in the Gauss–Laguerre summation (55) than is necessary to achieve the desired accuracy.

5. APPLICATION TO BOUNDARY LAYER FLOWS

The results of a series of test calculations are reported in this section for the two-dimensional Blasius boundary layer, in which the CPU time and accuracy for calculations with both anisotropic and isotropic Gaussian blob functions with various number of elements are compared as a function of Reynolds number. The elements are distributed on N_x rows along a flat plate of dimensionless length $L = 2$. A number N_y elements are distributed in each row in the direction normal to the plate, where the separation of the elements is set such that the farthest element control point lies at a distance $y = 6(2xL)^{1/2}/\mathrm{Re}_L^{1/2}$ from the plate ($\mathrm{Re}_L \equiv UL/\nu$), which corresponds to truncating the boundary layer when the similarity parameter $\eta \equiv y(U/2x\nu)^{1/2}$ exceeds 6. For anisotropic blob functions, the element radius R is set equal to $2\ \Delta x$ and the aspect ratio ε is set equal to $2\ \Delta y/R$, such that a uniform element overlap of 2 is maintained both tangential and normal to the plate. For isotropic blob functions, the elements radius R is set equal to the largest of $2\ \Delta x$ and $2\ \Delta y$.

The vorticity on each element control point is set using the standard similarity solution for the Blasius boundary layer (e.g., as given by White [18]). Using a representation of the form (9) for the vorticity field, we obtain a matrix equation for the element amplitudes Ω_n of the form

$$\omega_m = \sum_{n=1}^{N} W_{mn}\,\Omega_n, \tag{61}$$

where $\omega_m = \omega(\mathbf{x}_m, t)$ and $W_{mn} = f_n(\mathbf{x}_m - \mathbf{x}_n, R_n, \varepsilon_n)$. This matrix equation is, in general, ill-conditioned, such that solution of (61) with a fairly smooth vorticity field leads to large variations in amplitudes of nearby elements. Instead of solving (61) directly, we use an iterative scheme proposed by Marshall and Grant [10] to obtain a smooth fit to the vorticity field. In this iterative scheme, it is temporarily assumed that about each control point m, there exists a set of control points $n \in Q(m)$ for which the element amplitudes are nearly the same as that at control point m. Letting $P(m)$ denote the converse of $Q(m)$, the matrix equation (61) is approximated by

$$\omega_m = \Omega_m^{(q+1)} \sum_{n\in Q}^{N} W_{mn} + \sum_{n\in p} \Omega_n^{(q)}\, W_{mn}, \tag{62}$$

where q is an iteration index. The set $Q(m)$ typically includes 8–10 elements close to the given element m. The expression (62) usually coverges within about 6–8 iterations to a point where the maximum relative change in element amplitude is less than 10^{-6}. The error in vorticity due to the approximation (62) is of order $l^2\,\nabla^2\omega$, where l is the typical distance between neighboring elements (e.g., $l \cong \nabla y$ in the present application). For two-dimensional calculations, it then follows that the error due to the iteration (62) decreases with an increase in element number N roughly in proportion to $1/N$, which also agrees with our computational experience. Two examples showing the interpolated vorticity on a set of control points from the Blasius similarity solution (solid line) and the representation (61) (circles), after performing the iteration (62) using anisotropic elements, are given in Figs. 3a and b for cases with $N_y = 10$ and 40, respectively, and $N_x = 10$, and evaluated at $x = 1.1$. These figures generally indicate that the iterative procedure (62) yields an accurate fit to the vorticity field, although a small oscillation in vorticity is apparent in Fig. 3b very close to the wall, which occurs due to a sudden reduction in the amount of element overlap within a few element radii from the wall.

Once the element amplitudes are known, the induced velocity field is calculated using (39)–(40) for anisotropic elements and using (40)–(41) for isotropic elements. Both the velocity induced by the elements and that induced by image vorticity over the plate surface is included. An example of velocity profiles at $x = 1$ obtained from this procedure, using anisotropic Gaussian elements with $\mathrm{Re}_L = 1000$, is shown in Fig. 4 for $N_x = 10$ and values of N_y of 10 (dashed-double dotted curve), 20 (dashed curve), and 40 (solid curve). The maximum aspect ratios within the boundary layer for the anisotropic elements for the cases with $N_y = 10, 20, 40$ are $\varepsilon = 0.27, 0.13, 0.067$, respectively. The prediction of the Blasius similarity solution for the flat-plate boundary layer is shown in Fig. 4 using circular symbols. The velocity profiles in Fig. 4 are close to the similarity solution everywhere, except just above the boundary, where the computed velocity is observed to turn upwards so as to meet the boundary with a slope much less than that of the exact solution. It is recalled that since the image vorticity is of the opposite sign to that of the vorticity in the flow, a strong vorticity discontinuity occurs at the boundary in the exact Blasius boundary layer solution. The vortex blob representation smooths out the vorticity discontinuity and, hence, rounds the slope discontinuity in the velocity profile on the two sides of the plate. As shown in Fig. 4, the error associated with this smoothing can be delayed by decreasing the element aspect ratio while increasing the number N_y of elements used to discretize the flow in the direction normal to the wall. Nevertheless, it is clear that the smoothing of the vorticity field implicit in the vortex blob representation tends to introduce error (which may be considerable) in the calculation of wall slip velocity (which is sometimes used to specify the vorticity flux normal to the wall [7]) and wall shear stress. A method to eliminate this smoothing error is presented in the next section.

If isotropic elements are used for the boundary layer calculations at medium to high Reynolds numbers, the

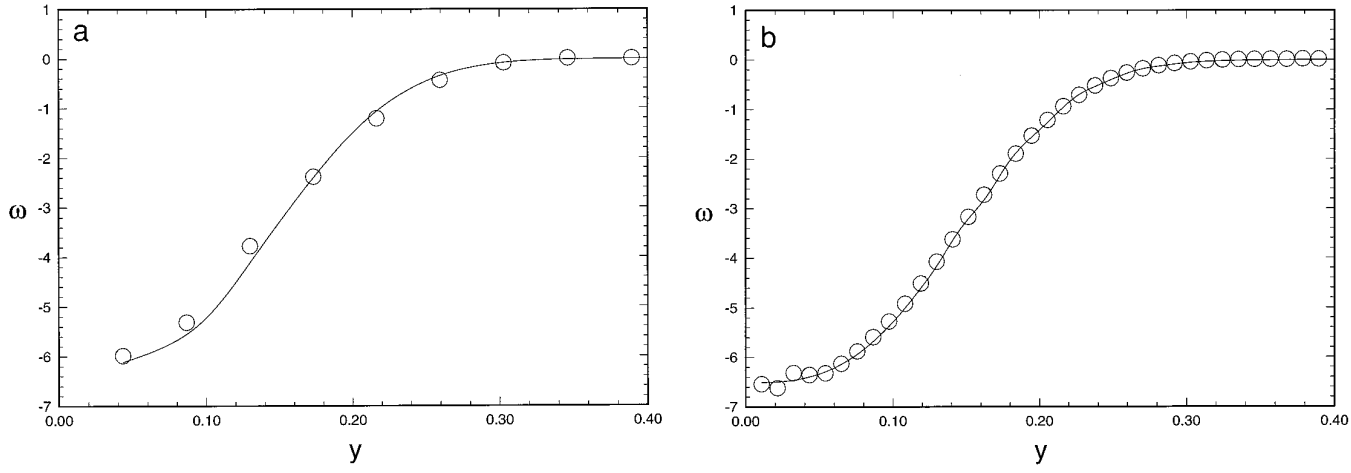

FIG. 3. Comparison of the vorticity profile at $x = 1.1$ for the Blasius similarity solution (solid curve) and the representation (61) (circular symbols), after using the iteration (62) to set the element amplitudes. Cases shown are for anisotropic elements with $N_x = 10$ and (a) $N_y = 10$ or (b) $N_y = 40$.

distance Δx between elements in the direction tangent to the boundary must be on the order of the element separation distance Δy normal to the boundary. If elements are placed out to a distance $y_{\max} = 6(2xL)^{1/2}/\mathrm{Re}_L^{1/2}$ in the Blasius boundary layer and the element radius is set by $R = 2\,\Delta y$, then at a position x the element radius is

$$R(x) = \frac{2y_{\max}}{N_y} = \frac{12(2xL)^{1/2}}{\mathrm{Re}_L^{1/2}\,N_y}. \tag{63}$$

The total number of isotropic elements required to cover the boundary layer in a two-dimensional calculation is then

$$N = N_y N_x = N_y \int_0^L \frac{2}{R(x)}\,dx = \frac{\sqrt{2}}{6}\,\mathrm{Re}_L^{1/2}\,N_y^2. \tag{64}$$

Predicted velocity profiles for calculations with isotropic elements are shown in Fig. 5 for a case with $\mathrm{Re}_L = 1000$, $N_y = 20$, and six different values of N_x, ranging from 20 to 300. The estimated value of N_x for this case from (64) is 150 for adequate coverage of the boundary layer. It is found that for values of N_x much less than the estimated value given by (64), the velocity profile will significantly

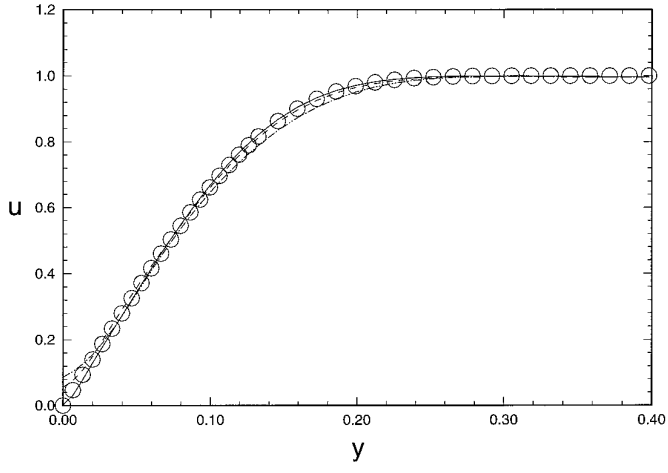

FIG. 4. Comparison of exact similarity solution for Blasius boundary layer at $x = 1$ (circular symbols) with computed results using anisotropic Gaussian vorticity elements, with $N_x = 10$ and three different values of cross-stream resolution: $N_y = 10$ (dashed-double dotted curve), 20 (dashed curve), and 40 (solid curve).

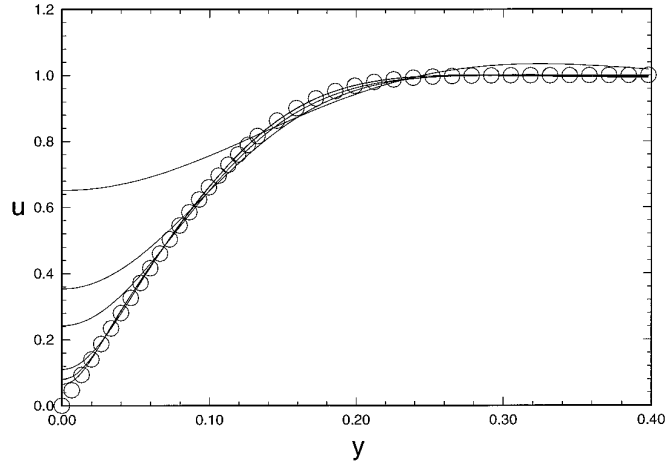

FIG. 5. Comparison of exact similarity solution for Blasius boundary layer at $x = 1$ (circular symbols) with computed results using isotropic Gaussian elements, with $N_y = 20$ and six different values of streamwise resolution: $N_x = 20, 36, 50, 100, 150, 300$. The computed slip velocity is observed to decrease monotonically as N_x is increased, such that at high N_x the results are nearly the same as for the calculations with anisotropic elements (Fig. 4, dashed curve).

deviate from the Blasius profile and yield a large wall slip velocity (as illustrated, for example, by the curves for $N_x = 20$, 36, and 50 in Fig. 5, which have slip velocities of 0.65, 0.35, and 0.24, respectively). As the value of N_x is increased to near or past the estimated value from (64), the velocity profiles (for $N_x = 100$, 150, and 300) converge to a curve which is very close to the dashed curve in Fig. 4, obtained using anisotropic elements with $N_x = 10$ and the same values of N_y and Re_L.

When the value of N_x is much lower than that given by (64) for isotropic elements, the element radii will be based on $2\Delta x (\gg 2\Delta y)$, such that the influence of the vorticity field of a single element may span a substantial amount of the boundary layer or even protrude out of the boundary layer. In this extreme case, not only is the smoothing error of the vorticity discontinuity at the wall greatly exaggerated, but the iteration scheme (62), together with the representation (61), tends to smooth out the vorticity field everywhere within the boundary layer, both lowering the peak vorticity at the wall and increasing the effective boundary layer thickness. This behavior is a consequence of the observation that the iteration (62) acts as a low-pass filter, which smears out vorticity fields with typical length scales much less than the element length scales in the x and y directions. Errors of this type do not arise with anisotropic elements, since the element radius and aspect ratio can be set independently to guarantee that the element length scale in the direction normal to the boundary remains small, compared to the boundary layer thickness, while still adequately covering the vorticity field by the element representation.

From the calculations shown in Fig. 5, the expression (64) seems to give a fairly reasonable estimate for the number of isotropic elements needed to resolve the Blasius boundary layer (on one side of the plate) in a two-dimensional flow. A comparison is now made between calculations with isotropic elements in which N_x is set by (64) and calculations with anisotropic elements in which N_x is set to some value $N_{x,\mathrm{ani}}$. Both calculations with isotropic and anisotropic elements have the same number N_y elements across the boundary layer in each row. The ratio $N_{\mathrm{iso}}/N_{\mathrm{ani}}$ of total number of isotropic elements to that of anisotropic elements required for a given two-dimensional calculation can then be expressed as a function of Reynolds number as

$$\frac{N_{\mathrm{iso}}}{N_{\mathrm{ani}}} = \frac{\sqrt{2}}{6}\,\mathrm{Re}_L^{1/2}\,\frac{N_y}{N_{y,\mathrm{ani}}}. \tag{65}$$

For a three-dimensional calculation, N is of the order $N_y N_x^2$ in (64), so the ratio in (65) becomes

$$\frac{N_{\mathrm{iso}}}{N_{\mathrm{ani}}} = \frac{1}{18}\,\mathrm{Re}_L\,\frac{N_y^2}{N_{x,\mathrm{ani}}}. \tag{66}$$

We have reported in Section 3 that calculation of the induced velocity at a typical point P requires 9.3 times longer for anisotropic Gaussian elements than for isotropic elements. The ratio of the time required for a single time step with isotropic elements, t_{iso}, to that required with anisotropic elements, t_{ani}, is then given (for a direct calculation) by

$$\frac{t_{\mathrm{iso}}}{t_{\mathrm{ani}}} = \left(0.11\,\frac{N_{\mathrm{iso}}}{N_{\mathrm{ani}}}\right)^2. \tag{67}$$

In our calculations for the Blasius boundary layer with anisotropic elements, $N_{x,\mathrm{ani}} = 10$ and $N_y = 40$ gives fairly reasonable results, as shown in Figs. 4 and 5. For this case, $N_{\mathrm{ani}}/N_{\mathrm{iso}}$ in (65) is approximately equal to $\mathrm{Re}_L^{1/2}$. Substituting this estimate into (67) indicates that $t_{\mathrm{iso}}/t_{\mathrm{ani}}$ for this example is about $\mathrm{Re}_L/100$. For high Reynolds number near-wall flows, the anisotropic elements clearly offer substantial time reduction.

Further advantages of using anisotropic elements arise with the use of an accelerated algorithm, such as that of Greengard and Rohklin [11]. In this case, both anisotropic and isotropic elements can be treated as point vortices when the velocity is calculated at points sufficiently far away, such that for an $O(N)$ algorithm $t_{\mathrm{iso}}/t_{\mathrm{ani}}$ would be equal to $N_{\mathrm{iso}}/N_{\mathrm{ani}}$ in the indirect part of the velocity computation (i.e., box–box or box–element interaction) and (67) would apply only to the direct part of the velocity computation (i.e., element–element interaction). One of the major limiting factors with accelerated algorithms based on multipole expansions is the amount of memory required, which can increase nearly as N^2 (multiplied by a small factor) in order to store the level of interaction between each box and other boxes. By reducing the number of elements with use of anisotropic blob functions, the memory requirements can also be substantially reduced.

6. IMPROVEMENT OF NEAR-WALL FLOW CALCULATION WITH ANISOTROPIC VORTICITY DOUBLETS

In the previous section, we found that the vortex blob representation smooths the vorticity discontinuity at the wall and leads to an error in calculation of wall slip velocity and shear stress. While the error was shown in Fig. 4 to become less severe as the number of elements spanning the boundary layer increases, even for values of N_y as large as 40 there is substantial error in the calculated wall shear stress (e.g., see the solid curve in Fig. 4). This smoothing error can be largely avoided, however, by placing doublet-type elements along the wall. Doublet-type elements are formed of two vorticity patches of opposite signs, where the vorticity within the doublet changes discontinuously

across its centerline. By placing doublet-type elements along the wall, the required vorticity discontinuity at the wall can be enforced.

As an example, the distribution function for the doublet equivalent to the two-dimensional Gaussian blob (22) is simply

$$h(x, y) = [2H(y) - 1] \exp[-(x^2 + y^2/\varepsilon^2)], \qquad (68)$$

where $H(y)$ is the step function ($H(y) = 1$ for $y > 0$ and $H(y) = 0$ for $y < 0$). We can again integrate the governing equations (17) for I_1 and I_2 in the positive $x - y$ quadrant, but now we require that the velocity be entirely in the x-direction on *both* $x = 0$ and $y = 0$, such that there is no flow over the doublet centerline. The boundary conditions (16) are thus changed for the vorticity doublet to

$$\left.\frac{\partial I}{\partial x}\right|_{x=0} = 0, \quad \left.\frac{\partial I}{\partial x}\right|_{y=0} = 0. \qquad (69)$$

An expression for I_2 satisfying $(17)_2$ is given still by (24), but now the boundary condition (25) on I_1 along $y = 0$ becomes

$$\left.\frac{\partial I}{\partial x}\right|_{y=0} = -\left.\frac{\partial I_2}{\partial x}\right|_{y=0} = 2\pi\varepsilon^2 x\, e^{-x^2}. \qquad (70)$$

A harmonic function I_1 which satisfies the boundary conditions (70) and $(69)_1$ can be obtained following an approach similar to that described in Section 3 for two-dimensional vorticity blobs. Combining this solution with the expression (24) for I_2 and differentiating with respect to x and y gives

$$\frac{\partial I}{\partial x} = 2\pi\varepsilon^2(xa - yb) + 2\pi\varepsilon^2 x\, e^{-x^2}\left[\sqrt{\pi}\frac{y}{\varepsilon}\operatorname{erfc}\left(\frac{y}{\varepsilon}\right) - e^{-y^2/\varepsilon^2}\right], \qquad (71a)$$

$$\frac{\partial I}{\partial y} = 2\sqrt{\pi}\varepsilon^2 - 2\pi\varepsilon^2(ya + xb) - \pi^{3/2}\varepsilon\, e^{-x^2}\operatorname{erfc}(y/\varepsilon), \qquad (71b)$$

where a and b are the real and imaginary parts, respectively, of the Faddeeva function $w(z)$. It is noted that only the $\partial I_2/\partial y$ term in (71b) is of $O(\varepsilon)$, the other terms in (71a) and (71b) being of $O(\varepsilon^2)$. The leading order approximation in ε for the gradients of $I(x, y)$ for a highly anisotropic Gaussian vorticity doublet is therefore simply

$$\frac{\partial I}{\partial y} = -\pi^{3/2}\varepsilon\, e^{-x^2}\operatorname{erfc}(y/\varepsilon) + O(\varepsilon^2), \quad \frac{\partial I}{\partial x} = O(\varepsilon^2). \qquad (72)$$

Sample calculations have been performed for the Blasius boundary layer using a single anisotropic doublet at the wall below each row of elements. The normalization constant A for doublets of the form (68) is the same as that given in (23) for Gaussian vorticity blobs. The amplitude of the doublet is fit using the same interation formula (62) as for any other element. We find that with use of vorticity doublets at the wall, the no-slip condition is much more closely satisfied and the slope of the velocity profile near the wall is much smoother than without the vortex doublets. An example comparing the velocity profile calculated both with and without vorticity doublets is shown in Fig. 6 for anisotropic elements with $N_x = N_y = 10$. Even though the number of elements used in this calculation is quite a small ($N = 100$), the velocity profile calculated with surface vorticity doublets agrees extremely well with the Blasius similarity solution right up to the wall.

7. CONCLUSIONS

In this paper, a method is presented for obtaining approximate expressions for the velocity induced by highly anisotropic, smooth vorticity elements, in which element aspect ratio is used as a small parameter. The method is illustrated for anisotropic Gaussian elements in both two and three dimensions. In the two-dimensional case, the induced velocity for the Gaussian element is expressed in terms of the Faddeeva function $w(z)$, which can be obtained using an efficient algorithm available in Ref. [15]. In the three-dimensional case, the induced velocity for the Gaussian element is obtained in terms of 2 one-dimen-

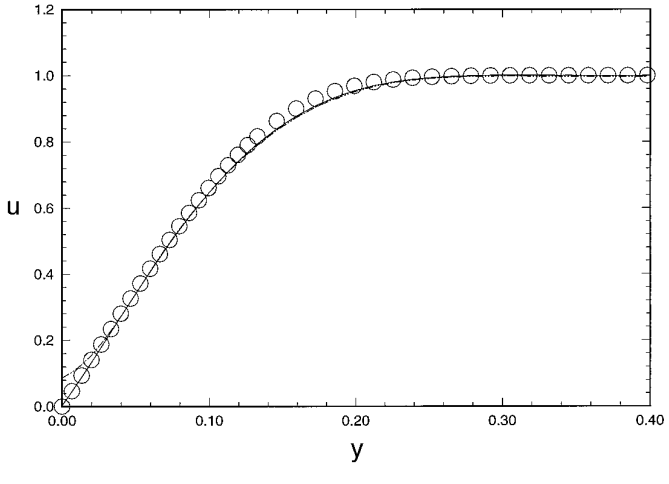

FIG. 6. Comparison of computed results for the Blasius boundary layer at $x = 1$ for calculations with vorticity doublets at the surface (solid curve) and without vorticity doublets (dashed-double dotted curve). The calculations are for $N_x = N_y = 10$, and the results of calculations with vorticity doublets are found to compare very well with the exact similarity solution (circular symbols).

sional integrals which can be efficiently evaluted numerically using Gauss–Laguerre quadratures.

Tests comparing accuracy and CPU time for calculations of the Blasius boundary layer using both anisotropic and isotropic blob functions were performed. It is found that with a given resolution of the vorticity across the boundary layer, the velocity profiles calculated using isotropic blob functions approach those obtained with anisotropic blob functions as the separation of isotropic elements along the wall becomes sufficiently small. The ratio of the number of isotropic elements to the number of anisotropic elements required to resolve a flow with a given accuracy is found to increase in proportion to the square-root of the Reynolds number for two-dimensional flows and in proportion to the Reynolds number for three-dimensional flows. Even though induced velocity calculation at a given field point requires nearly 10 times as long with an anisotropic Gaussian element as with an isotropic element, the decrease in the number of elements required can result in significant CPU time reduction for high Reynolds number near-wall flows.

One shortcoming of the vortex blob representation for boundary layer calculations, for both anisotropic and isotropic elements, is that the discontinuity which occurs at the wall between the real vorticity field and the image vorticity field is smoothed by the vorticity representation in terms of overlapping blobs. This smoothing yields a velocity profile which turns upwards just above the wall, causing an error in the calculation of slip velocity and wall shear stress. This difficulty can be avoided by placing vorticity doublets, formed of vorticity regions of opposite signs with a vorticity discontinuity at the centerline, along the wall. Calculations using these vorticity doublets on the wall, together with anisotropic elements with the flow, have been found to yield velocity profiles in excellent agreement with the exact Blasius solution using a very small number of elements.

There are still a number of unresolved issues in the development of deterministic vortex methods, including the development of implicit diffusion methods which are accurate for irregularly spaced control points, development of methods for adding or moving control points to regions into which the vorticity diffuses, and continuing questions regarding vorticity boundary conditions at a wall. In the current paper we have addressed only one of the problems associated with deterministic vortex methods: namely, given a highly anisotropic vorticity distribution (possibly along a wall), how can one accurately compute the induced velocity field using a minimum number of smooth elements. The accuracy of computational methods which make use of anisotropic smooth elements will depend critically on the choices made for the three issues listed above. Our current computational method resolves these three issues in ways that are very different than those which can be found in the available literature, and for this reason dynamic simulations using the anisotropic elements developed here will therefore be presented in a separate paper.

ACKNOWLEDGMENTS

Research support for J.S.M. was provided by the U.S. Army Research Office under Grant Number DAAH04-94-G-0378 with the University of Iowa, by an Old Gold Summer Fellowship from the University of Iowa, and by the ASEE/Navy Summer Faculty Research Program during the summer of 1994. Research support for J.R.G. was provided by the U.S. Office of Naval Research under Grant Number N0001493WX22029 and by internal funding from the Naval Undersea Warfare Center, Division Newport.

REFERENCES

1. A. J. Chorin, *J. Comput. Phys.* **27,** 428 (1978).
2. S. Huyer, J. R. Grant, and J. S. Uhlman, AIAA Paper 94-0075, 1994 (unpublished).
3. P. S. Bernard, *J. Comput. Phys.* **117,** 132 (1995).
4. Z. H. Teng, *J. Comput. Pnys.* **46,** 54 (1982).
5. O. M. Knio and A. F. Ghoniem, *J. Comput. Phys.* **86**(1), 75 (1990).
6. G. S. Winckelmans and A. Leonard, *J. Comput. Phys.* **109,** 247 (1993).
7. P. Koumoutsakos, A. Leonard, and F. Pépin, *J. Comput. Phys.* **113,** 52 (1994).
8. J. T. Beale and A. Majda, *Math. Comput.* **39**(159), 1 (1982).
9. J. T. Beale and A. Majda, *Math. Comput.* **39**(159), 29 (1982).
10. J. S. Marshall and J. R. Grant, *J. Fluid Mech.,* **103,** 83 (1996).
11. L. Greengard and V. Rokhlin, *J. Comput. Phys.* **73,** 325 (1987).
12. E. A. Novikov, *Sov. Phys. JETP* **57**(3), 566 (1983).
13. I. S. Gradshteyn and I. M. Ryzhik, *Tables of Integrals, Series and Products* (Academic Press, Orlando, FL, 1980).
14. V. N. Faddeeva and N. N. Terent'ev, "Tables of Values of the Function $w(z) = e^{-z^2}(1 + 2i/\sqrt{\pi}\int_0^z e^{t^2}\,dt)$ for Complex Argument," (*Gosud. Izdat. Teh.-Teor. Lit.,* Moscow, 1954); English transl. (Pergamon, Press, New York, 1961).
15. G. P. M. Poppe and C. M. J. Wijers, *ACM Trans. Math. Software* **16**(1), 38 (1990).
16. M. Abramowitz and I. A. Stegun, *Handbook of Mathematical Functions* (Dover, New York, 1965).
17. W. H. Press, B. P. Flanery, S. A. Teukolsky, and W. T. Vettering, *Numerical Recipes,* 2nd ed. (Cambridge Univ. Press, Cambridge, 1992).
18. F. M. White, *Viscous Fluid Flow* (McGraw–Hill, New York, 1974), p. 265.